Multimedia Tools and Applications
https://doi.org/10.1007/s11042-020-10049-7

Underwater image restoration based on secondary guided transmission map

Jingchun Zhou[1] · Zhenzhen Liu[1] · Weidong Zhang[1] · Dehuan Zhang[1] · Weishi Zhang[1]

Received: 18 October 2019 / Revised: 10 September 2020 / Accepted: 7 October 2020
Published online: 30 October 2020

Abstract
The color distortion and low contrast of underwater images are caused by the absorption of light by water and the scattering of suspended particles. So, we propose an underwater image restoration method based on secondary guided transmission map, which can effectively restore the color, visibility and natural appearance of underwater image. We use improved guided filter to refine the transmission map. Firstly, the rough transmission map is decomposed into the basic image and the detail image by the guided filter. And then refined transmission map is reconstructed after processing the images respectively. Finally, auto level processing is conducted on the restored image to improve the contrast of the image. In order to evaluate the effectiveness of our method, qualitative and quantitative comparisons and application test are carried out. Experimental results demonstrate that compared with several state-of-the-art methods, the proposed method can get genuine color, natural appearance, and the improvement of visibility and contrast.

Keywords Underwater image restoration · Underwater imaging · Guided filter · Auto level

1 Introduction

In the case of shortage of land resources, marine resources protection and development is a far-reaching strategic choice. In recent years, underwater images have been widely used in marine energy exploration, marine ecological protection, marine military and other fields [5, 20]. However, underwater image appears the problems of color distortion, low contrast and detail loss because of the selective absorption of light by water and scattering of suspended particles.

✉ Weishi Zhang
teesiv@dlmu.edu.cn

Jingchun Zhou
630790387@qq.com

[1] Dalian Maritime University, Dalian, China

Many physical model-based restoration methods are proposed to deal with the degradation of the underwater image.

The physical model-based restoration method is to establish an imaging model for underwater image degradation process. By estimating the parameters, a clear underwater image can be inverted. Physical model-based underwater image restoration methods can be divided into four categories: special hardware, polarization imaging, optical characteristics and prior knowledge-based methods. The first category is the methods of using special hardware. For example, He et al. [7] adopted optical/laser sensing technology to capture turbid underwater images. Although the methods effectively improve the imaging quality, the special equipment is very expensive and the cost of implementation is high, which has limitations.

The second class includes the methods based on polarization imaging [11, 13]. Huang et al. [13] considered the polarization effect of the object, and obtained good experimental results. The details of the object are highlighted, but during the process of processing the image, it is necessary to select the background area without object manually. Hu et al. [11] considered the conditions of non-uniform optics field, and proposed a method of underwater image restoration based on polarization imaging, which could effectively improve the image quality. All of the above methods can improve the contrast, but the operation is complex, and the practicability is weak.

The third class is the methods based on optical properties. Hou et al. [10] combined underwater optical properties with traditional image restoration, which assumed that the blurring of underwater images is caused by light scattering from water and suspended particles. The method used deconvolution to restore underwater image by estimating illumination scattering parameters. Zhao et al. [30] considered that the degradation of underwater image is related with the optical properties of water, obtained the inherent optical properties of water through the background color of underwater images, which restore a clear underwater image by inversion of the degradation process. Li et al. [17], based on the minimum information loss and optical properties of underwater imaging, proposed an underwater image visibility and color restoration method, which has a natural color and improved contrast and visibility. The scattering coefficient is related with different water types, so the above method is only applicable to specific water types.

The fourth class of methods is based on prior knowledge. In the types of prior knowledge, dark channel prior (DCP) algorithm [8] is the most common one, which is originally used for outdoor scene dehazing. Dark channel prior is the basis of many underwater image restoration studies. Drews et al. [3] only considered green and blue channels to restore the quality of underwater images based on DCP. Chiang and Chen [2] proposed an underwater image restoration method combining image dehazing and wavelength compensation. The classical DCP algorithm is improved, which can improve the clarity of underwater image and reduce the influence of artificial light. Galdran et al. [4] found that the reciprocal of the red component increased with the distance to the camera, so the red channel is introduced to restore the color with short wavelength, which enhanced the contrast and realized color correction. Peng et al. [26] proposed an underwater scene depth estimation method based on image blur and light absorption, which can restore and enhance underwater images in the image formation model (IFM), and this method can estimate the depth of underwater scene more accurately. Mathias et al. [24] proposed a method of underwater image restoration based on diffraction bounded optimization algorithm of DCP, which can obtain better clarity. In general, dark channel prior is adopted to obtain the transmission map, but the block artifacts produced due to the local minimization operation. In order to solve the block artifacts, a local linear image filter proposed by He et al. [9], which can effectively smooth the block artifacts, preserves the edge, and avoids the gradient reversal effect. Therefore, it has broad application prospects in image dehazing [31], image restoration, image enhancement and other fields.

In conclusion, we propose an underwater image restoration method based on secondary guided transmission map. Firstly, the red channel is inverted, and the dark channel prior is used in the inverted image to get the background light. And then, the saturation is added to obtain a rough transmission map, and then the improved guided filter is used to refine the transmission map. Finally, the underwater image is restored. The major contributions of this paper include:

1) Our method proposes secondary guided filtering to refine the transmission map;
2) In order to improve the contrast, the proposed method adopts the auto level method to stretch the contrast of the restored image.

The rest of the paper is organized as follows. Section 2 introduces relevant theories, including underwater optical imaging model, guided filter, and red dark channel prior. In Section 3, the proposed method and specific steps are introduced. Section 4 evaluates and analyses the experimental results, by qualitative and quantitative comparisons and application test. Section 5 is the conclusion of this paper.

2 Related theory

In this section, we briefly introduce the underwater optical imaging model, guided filter, and red dark channel prior, which are the basis of our method.

2.1 Underwater optical imaging model

According to the underwater imaging model of Jaffe-McGlamery [25], the light received by the underwater camera consists of three linear components: direct component, forward scattering component and back scattering component. As shown in Fig. 1.

The direct component is the reflected light of the object does not scatter into the camera; Forward scattering component is the part of the object-reflected light that enters the camera

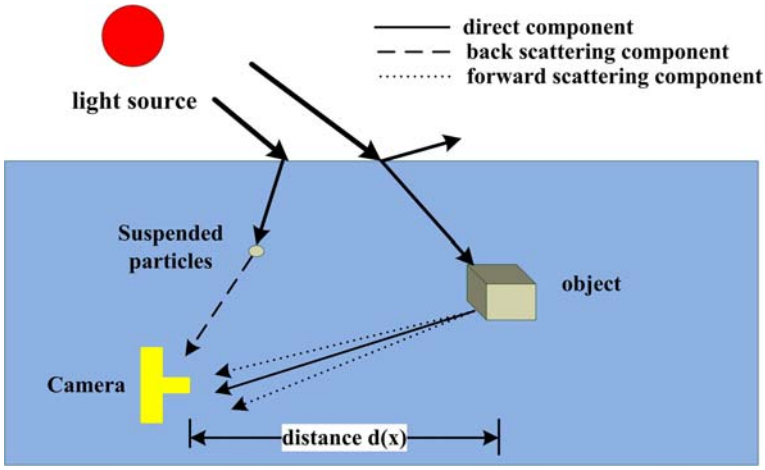

Fig. 1 Underwater optical imaging model

after scattering at a small angle; Back scattering component is the part of background light that enters the camera after scattering by suspended particles. When the distance between the object and the camera is small, and the forward scattering component is neglected, the underwater optical imaging model can be simplified [18] as:

$$I^c(x) = J^c(x)t^c(x) + A^c(1-t^c(x)), c\in\{r,g,b\} \tag{1}$$

where $I^c(x)$ is the original image, $J^c(x)t^c(x)$ represents the direct component, $A^c(1-t^c(x))$ denotes the background light scattering component, A^c indicates the background light, and $t^c(x)$ represents the transmission map.

When light propagates in water, it decays exponentially [29]. We assume that the water medium is uniform, the transmission map is defined expressed as:

$$t^c(x) = \exp(-\beta^c d(x)), c\in\{r,g,b\} \tag{2}$$

where β^c represents attenuation coefficient, $d(x)$ represents the depth of the scene.

2.2 Guide filter

Guided filter is an edge-preserving filter [9, 22], which can effectively smooth the image and preserve the edge. Formula as:

$$q = guidefilter(p, I, r, \varepsilon) \tag{3}$$

where r is the size of the filter window, ε represents the regularization parameter to preventing a_k from being too large, I is the guide image, p represents the filtered input image and q indicates the output image. There is a linear relationship between I and p, as follows:

$$q_i = a_k I_i + b_k, \forall i\in\omega_k \tag{4}$$

where the window is centered on a pixel k, the window size is $r\times r$, (a_k, b_k) is a constant coefficient in ω_k, by minimizing the cost function, we get the constant coefficient (a_k, b_k). Pixel i is contained in multiple windows covering i, different window ω_k, a different value of q_i, average all the possible values of q_i. The output image q can be written as:

$$q_i = \frac{1}{|\omega|}\sum_{k\in\omega_k}(a_k I_i + b_k) = \overline{a}_k I_i + \overline{b}_k \tag{5}$$

Due to the limitation of local linear features of guided filter and the minimization cost function, the output image not only obtains the various details of the guided image but also retains the overall features of the original image.

2.3 Red Dark Channel prior

According to the underwater optical imaging model, background light and transmission map are the key factors of image restoration. The dark channel prior proposed by He et al. [8] effectively solves the problem of estimating the background light and transmission map of outdoor haze images, so many scholars apply this method to underwater image restoration. DCP theory indicates that for outdoor fog-free image except for the sky area, at least one color channel in the local area has a very low value, which close to 0.

$$J^{\text{dark}}(x) = \min_{c\in\{r,g,b\}} \left(\min_{y\in\Omega(x)} \left(J^c(y)\right) \right) \to 0 \tag{6}$$

where $J^{\text{dark}}(x)$ represents the dark channel of the haze-free image, $\Omega(x)$ represents a local patch which centers on x, $J^c(y)$ represents haze-free images for each channel.

In the DCP, the transmission map is obtained by the minimization operation is performed at both ends of Eq. (1):

$$\min_c \left(\min_{y\in\Omega(x)} \frac{I^c(y)}{A^c} \right) = t(x) \min_c \left(\min_{y\in\Omega(x)} \frac{J^c(y)}{A^c} \right) + 1 - t(x) \tag{7}$$

According to the DCP theory, the first term on the right side of the Eq. (7) tends to 0, and the transmission map as:

$$t(x) = 1 - \min_c \left(\min_{y\in\Omega(x)} \frac{I^c(y)}{A^c} \right) \tag{8}$$

Although underwater images model is similar to haze imaging model, due to the situation that different wavelengths of light have different degrees of attenuation in underwater environment, and red light with longer wavelength decays faster in water, so the direct use of dark channel prior will lead to the over-estimation of transmission map. If the red channel value is not taken into account [27], estimating the transmission map only through blue and green channels will result in a smaller transmission map.

Considering the fastest attenuation of red light, the imaging model is split into three channels in Galdran [4] algorithm, and the red channel is inverted. As follows:

$$\begin{aligned} 1 - I^R &= t^R\left(1 - J^R\right) + \left(1 - t^R\right)\left(1 - A^R\right), \\ I^G &= t^G J^G + \left(1 - t^G\right)A^G, \\ I^B &= t^B J^B + \left(1 - t^B\right)A^B \end{aligned} \tag{9}$$

where $I = (I^R, I^G, I^B)$, $J = (J^R, J^G, J^B)$ are the original image (degraded image) and the restored image respectively. Eq. (9) is equivalent to Eq. (1).

Combined with a DCP and underwater imaging model, Galdran et al. [4] proposed the red dark channel prior (RDCP):

$$J^{RED}(x) = \min\left(\min_{y\in\Omega(x)} \left(1 - J^R(y)\right), \min_{y\in\Omega(x)} \left(J^G(y)\right), \min_{y\in\Omega(x)} \left(J^B(y)\right) \right) \to 0 \tag{10}$$

where J represents a clear image.

3 Proposed method

In this section, we proposed an underwater image restoration method based on the secondary guided transmission map, which can be mainly divided into five steps:(1) background light estimation; (2) saturation estimation; (3) transmission map estimation; (4) image restoration; (5) contrast stretch. Among them, Step (3) transmission map estimation is refined by secondary guided filtering, and the specific operation are: the rough transmission map is decomposed into the basic image and the detail image by the guided filter; to enhance image details, the basic image is

processed by Laplace filter; in order to solve the block effect and maintain the contour edge information, the detail image is processed by guided filtering; A linear fusion of the processed basic image and detail image are reconstructed to obtain the refined transmission map.

The proposed method flowchart is shown in Fig. 2.

Table 1 presents a summary of the proposed underwater image restoration method. The red dark channel map is calculated using Step (1), followed the background light is estimated in Step (2). The saturation and coarse transmission map are estimated in Steps (3) and (4), respectively. By using secondary guided filter based on Step (5). Step (6) to restore underwater images. The final restored image is obtained by using Contrast stretch based on Step (7).

3.1 Background light estimation

The state-of-the-art algorithms usually acquire background light A based on the pixels related to a single image. In He [8] algorithm, the top 0.1% pixels with the largest pixel value are selected in the dark channel image and these pixels are corresponded to the haze image, and the pixel with the highest value (for pixel) is selected as atmospheric light A.

We propose a similar method is adopted to apply the dark channel prior to the image after the red channel inversion. And that is, we obtain the background light from the red dark channel image. The specific steps are: We calculate the red dark channel of the original image I, and use the top 10% of the brightest pixels in the red dark channel. In 10% pixels, we select the pixel with low red content and record their location x_0 (see Fig. 3). In the original image, this position $I(x_0)$ is the background light, obtaining A^R, A^G, A^B by Eq. (11).

$$A = \left(I^R(x_0), I^G(x_0), I^B(x_0)\right) \tag{11}$$

3.2 Saturation estimation

When the artificial light source exists, the intensity of the pixels in the illumination area is greatly increased. According to Eq. (10), the transmission map of the area is smaller, which affect the restoration effect. The proposed method reduces the effect of artificial light source via adding saturation to RDCP.

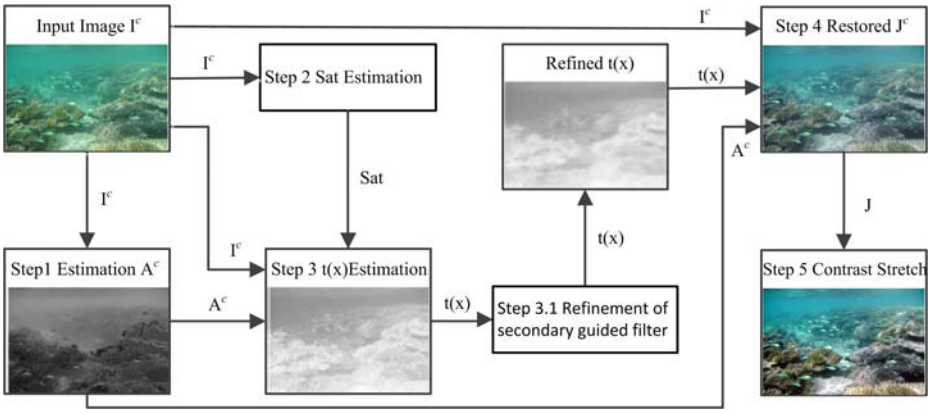

Fig. 2 Flowchart of the proposed method

Table 1 Summary of the proposed method

Input: underwater image I
Output: restored image J
(1) Red dark channel map using Eq. (10), obtain I_{red}.
(2) Estimate background light A^c using Eq. (11).
(3) Estimate Saturation Sat using Eq. (12).
(4) Estimate coarse transmission map $t(x)$ using Eq. (14).
(5) Obtain refine transmission map $t(x)$.
(6) Restored underwater image J^c using Eq. (23).
(7) Obtain final restored image J using Eq. (24).

In the image, the saturation of a pixel indicates the purity of the chromaticity of in the pixel, when the chromaticity of a pixel is pure, its saturation is high. When illuminated by an artificial light source, the saturation of the pixels in the illuminated scene will decrease because the light source used is usually white and contains all visible bands. The saturation is as follows:

$$\mathrm{Sat}(I) = \frac{\max\left(I^R, I^G, I^B\right) - \min\left(I^R, I^G, I^B\right)}{\max\left(I^R, I^G, I^B\right)} \tag{12}$$

When there is artificial lighting, the visible light in each band of the light source will make certain compensation for the color of the pixel, so that the value of the three components of the pixel color tends to be uniform. In this case, the saturation closes to zero.

After adding the saturation component, the RDCP is modified into:

$$J^{RED-SAT}(x) = \min\left(\min_{y\in\Omega(x)}\left(1-J^R(y)\right), \min_{y\in\Omega(x)}\left(J^G(y)\right), \min_{y\in\Omega(x)}\left(J^B(y)\right), \min_{y\in\Omega(x)}\mathrm{Sat}(y)\right)\to 0 \tag{13}$$

When the illuminated area of an artificial light source is located in the near scene, the estimated transmission map is too small according to Eq. (10) to judge that the area is located in the far scene, as shown in Fig. 4b, the illumination area presents reddish chromatic artifacts due to the incorrect scene estimation. When Eq. (13) estimates the transmission map, the saturation tends to zero due to the use of artificial light source, which weakens the influence of high brightness value on the estimation of the transmission map and it correctly judges as a near scene, and improves the quality of image restoration by Fig. 4c.

We can observe that restored images (without contrast stretch processing) using saturation prior has better visual effect by Fig. 4.

When there is no artificial light source in the scene, the saturation of the pixel must be far from 0. Adding a prior saturation does not affect the estimation of transmission map. Eq. (13) is used in all cases.

Fig. 3 Red dark channel in the background light selection (**a**) Original image (**b**) Red dark channel of the original image (**c**) Selection position of background light (small red point marked in the figure) (**d**) Final restoration image

(a) (b) (c)

Fig. 4 The result of image considering or not considering saturation (**a**) Image with artificial light source (**b**) Restored image without considering saturation prior (**c**) Restored image with considering saturation prior

3.3 Transmission map estimation

After the background light and saturation are estimated, it is assumed that the transmission map is locally constant. According to the RDCP, $t(x)$ can be calculated as:

$$t(x) = 1-\min\left(\frac{\min\limits_{y\in\Omega(x)}\left(1-I^R(y)\right)}{1-A^R}, \frac{\min\limits_{y\in\Omega(x)} I^G(y)}{A^G}, \frac{\min\limits_{y\in\Omega(x)} I^B(y)}{A^B}, \lambda \min\limits_{y\in\Omega(x)} \mathrm{Sat}(y)\right) \tag{14}$$

where $\lambda \in [0,1]$, it can be adjusted manually, the value in this paper is 0.6.

The coefficient λ is used for saturation estimation. The artificial light source image is used for illustration, as shown in Fig. 5. When the coefficient is 0.5, the background color of the restored image (without contrast stretch processing) is a little greener; When it is 0.7, the background color of the restored image is little darker and redder; When it is 0.6, the visual effect of the restored image is better, and finally 0.6 is selected.

In the underwater imaging process, different wavelength attenuation coefficients are different, red wavelength attenuation is the fastest, followed by green and blue. Therefore, the transmission map is different. Galdran et al. [4] pointed out the relationship between the transmission map of three channels:

$$\begin{aligned} t^R(x) &= 1-\min\left(\frac{\min\limits_{y\in\Omega(x)}\left(1-I^R(y)\right)}{1-A^R}, \frac{\min\limits_{y\in\Omega(x)} I^G(y)}{A^G}, \frac{\min\limits_{y\in\Omega(x)} I^B(y)}{A^B}, \lambda \min\limits_{y\in\Omega(x)} \mathrm{Sat}(y)\right), \\ t^G(x) &= e^{-\beta^G d(x)} = \left(e^{-\beta^R d(x)}\right)^{\frac{\beta^G}{\beta^R}} = \left(t^R(x)\right)^{\lambda_G}, \\ t^B(x) &= e^{-\beta^B d(x)} = \left(e^{-\beta^R d(x)}\right)^{\frac{\beta^B}{\beta^R}} = \left(t^R(x)\right)^{\lambda_B} \end{aligned} \tag{15}$$

According to Eq. (15), the transmission map of red channel can be obtained. λ_G and λ_B are the attenuation coefficient ratios of green-red and blue-red, the corresponding transmission map can be obtained by calculation of the attenuation coefficient ratio.

Since the local minimization operation is used in the calculation of the transmission map, this result in the block artifacts. Generally soft matting [16] or guided filter [9] will be used to refine the coarse transmission map. Although the transmission map optimized by soft matting method has a good effect, it is not suitable for real-time image processing due to its large

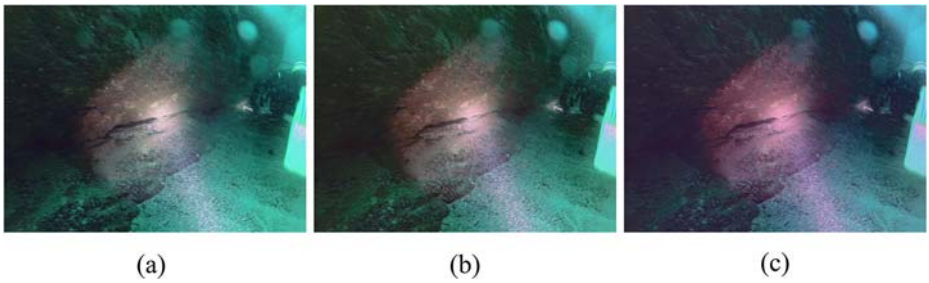

Fig. 5 The restored images of different lambda (**a**) λ value is 0.5 (**b**) λ value is 0.6 (**c**) λ value is 0.7

amount of computation, high complexity and long running time. The proposed method employs improved guided filter to refine transmission map, and the refining effect is excellent as shown in Fig. 6f, which has fast operation speed and good processing effect.

3.3.1 Improved guided filter

This paper proposed an edge-preserving decomposition method based on the guided filter. Guided filter decomposes the coarse transmission map into basic image and detail image. Since the guide filter retains the edge of the image while removing texture details, it makes the basic image have both low frequency and strong edge. Therefore, the basic image contains the large-scale information of the original image, and the detail image contains the contour details of the original image. The basic image is processed by Laplace filter, and the detailed image is processed by the guided filter, the processed basic image and detailed image are added to complete the reconstruction, and the refined transmission map is obtained. The steps are as follows:

1) Guided filter decomposes the input image into basic image and detail image.

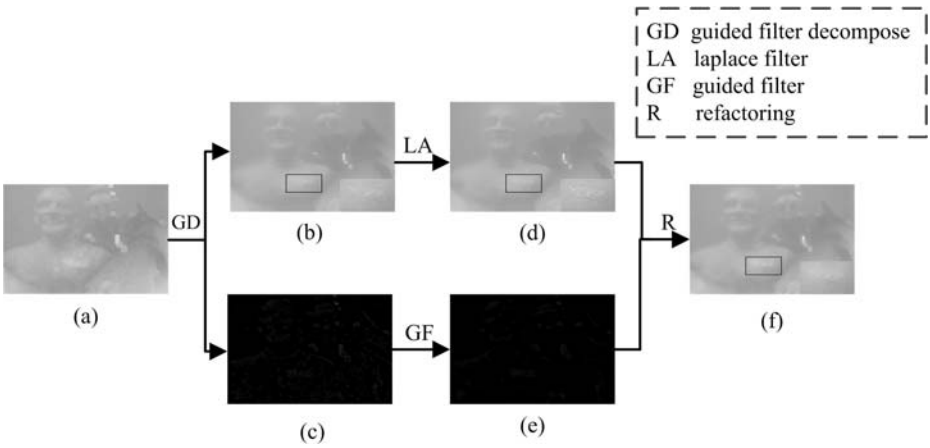

Fig. 6 Refined transmission map (**a**) Coarse transmission map (**b**)Basic image (**c**) Detail image(**d**) Laplace filter after the basic image (**e**)Guide filter after detail image (**f**) Reconstructed image (refined transmission map)

$$u = guidefilter(t, I, r1, \varepsilon) \tag{16}$$

$$d = t - u \tag{17}$$

where I is a guide image. In this paper, the gray image of the original image is used as the guide image, t denotes the input image(coarse transmission map), u indicates the basic image obtained by filter, d represents the detail image, $r1$ is the size of the filter window, ε represents the regularization parameter.

2) The basic image is processed by a Laplace filter. The aim is to preserve the background information of the image while highlighting the small details of the image.

$$U = u * \text{Lap} \tag{18}$$

$$Lap = \begin{pmatrix} 0 & 1 & 0 \\ 1 & -4 & 1 \\ 0 & 1 & 0 \end{pmatrix} \tag{19}$$

where U is a basic image after the Laplace filter, Lap is a Laplace operator of 3×3, $*$ is a convolution operation. Laplace is a second-order differential linear operator. Its application can enhance the abrupt change of gray level in the image and weaken the slow change of gray level.

3) In order to eliminate the partial block artifacts of detail image, the guided filter is used to process detail image.

$$D = guidefilter(d, I, r2, \varepsilon) \tag{20}$$

where d represents the detail image, I is a guide image, $r2$ is the size of the filter window, ε represents the regularization parameter, D is a detailed image after the guided filter.

4) A linear fusion of basic detail image U and detail image D are used to reconstruct the refined transmission map.

$$t = U + D \tag{21}$$

The detailed image obtained by the decomposition of the first guide filter has a contour and detail information in addition to block artifacts, so it needs to be refined by the guide filter. However, the basic image has been refined block artifacts, Laplace filter is used to process the basic image to obviously enhance the details (see in Fig. 6d). The reconstructed image (Fig. 6f) contains both the contour details of the detailed image and the enhanced details of the basic

image. As shown in Fig. 6, the detailed contour information in Fig. 6f is clearer than that in Fig. 6b (ordinary guided filter), which indicates that our method is better than the transmission map obtained by the ordinary guided filter method.

3.4 Image restoration

After getting the transmission map and the background light, restored images need to be an inversion. In order to avoid overflow caused by a too low transmission map, a lower limit t_0 is added to t, and the typical value of t_0 is 0.1. The recovery formula is:

$$\begin{aligned} J^R(x) &= \frac{I^R(x)-A^R}{\max(t^R(x), t_0)} + A^R, \\ J^G(x) &= \frac{I^G(x)-A^G}{\max(t^G(x), t_0)} + A^G, \\ J^B(x) &= \frac{I^B(x)-A^B}{\max(t^B(x), t_0)} + A^B \end{aligned} \tag{22}$$

Since attenuation coefficients λ_G and λ_B hinge on the type of water, λ_G and λ_B are hard to determine. Using the same method as in [4], the estimated transmission map in Eq. (14) taken as the global transmission map. By adjusting the color components by weighting the background light, the incomplete effect of scattering removal caused by the unified calculation of the transmission map is reduced. The multiplication part of Eq. (1) is responsible for the restoration of the depth of the degraded image scene, and the additional part is responsible for removing the color casting. Color cast can be automatically removed due to the reciprocal of the background light. The final recovery formula is:

$$J^{\alpha}(x) = \frac{I^{\alpha}(x)-A^{\alpha}}{\max(t(x), t_0)} + (1-A^{\alpha})A^{\alpha} \tag{23}$$

where α represents the channel in RGB color space respectively, the restoration image cannot guarantee that the value is located in [0,1], so the minimum-maximum normalized intensity value is adopted to adjust its value range.

3.5 Contrast stretch

For better contrast stretching, the restored image value is adjusted to [0, 255]. The underwater image obtained by restoration has low contrast, which is processed with auto levels to enhance the brightness and contrast of the image, so as to achieve better visual effect. The level represents 256 grayscale levels, and the color level algorithm increases the visual effect by adjusting the brightness and darkness of the image to improve the contrast. The principle of adjusting the color level is that the original image histogram is redistributed on 256 grayscale levels, and the contrast is improved by stretching the gray level histogram of the image.

Auto level principle [12] is to automatically set the upper and lower thresholds according to the histogram of the original image. The gray value of the histogram which is less than the lower threshold is set as 0, and the gray value of the histogram which is greater than the upper threshold is set as 255. The part between the upper and lower thresholds is proportionally distributed to the gray level of [0, 255] through formula (24), and the new histogram is obtained as shown in Fig. 7.

$$X = \frac{255}{(x_{\max} - x_{\min})}(x - x_{\min}) \tag{24}$$

The setting method of the lower threshold is as follows: the number of pixels corresponding to 0 grayscale level and the number of pixels corresponding to the higher grayscale level is added successively until the cumulative value is greater than or equal to 0.5% of the total number of pixels of the whole image. The highest gray level in the gray level of the addition operation is set as the lower threshold. The upper threshold setting method is: the number of pixels corresponding to 255 grayscale level is added to the number of pixels corresponding to lower grayscale levels in turn until the cumulative value is greater than or equal to 0.5% of the total number of pixels in the whole image. The lowest gray level in the gray level of the addition operation is set as the upper threshold.

4 Experimental results and analysis

Our paper first introduces the role of contrast stretch, then evaluates the performance of the proposed method, qualitative comparison, quantitative comparison and application test are conducted respectively. In this experiment, the two free parameters r, ε of the guided filter have some influence on the refined transmission map. Using the default parameter setting, the window radius $r1$ is set to 22, $r2$ is set to 10, and the regularization parameter ε is set to 0.0001.

4.1 Verify the effectiveness of contrast stretch

To prove the effect of contrast stretching, we conduct ablation studies. As shown in Fig. 8, contrast stretching can effectively enhance image contrast and detail information, and the effectiveness of this step of contrast stretching can be further reflected by visual effects. In order to better prove, we adopt the visual edge method [6] to further verify. Fig. 8b shows the number of visible edges of the original image, Fig. 8d shows the number of visible edges of the image before contrast stretching. It can be seen from Fig. 8b and d that the red channel prior method can effectively increase the visible edges of the underwater image. But there are still

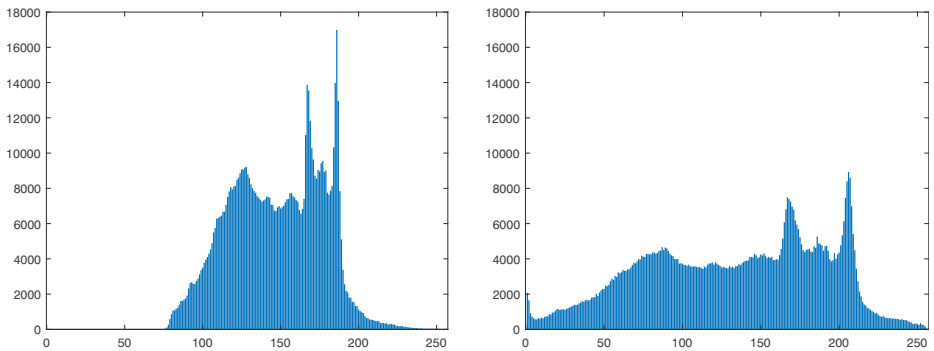

Fig. 7 Histogram (**a**) Histogram of the restored image (**b**) The final image histogram after auto level

some problems of low contrast and less detailed information in Fig. 8c. After contrast stretching, the number of visible edges in Fig. 8f increased significantly, indicating that the contrast stretching improves the image contrast and verifying the effectiveness of the contrast stretching.

4.2 Qualitative comparison

In this paper, we propose a method of underwater image restoration based on secondary guided transmission map and compare with the state-of-the-art methods. Methods used for comparison include dark channel prior (He) method [8], underwater single image transmission estimation (Drews) method [3], underwater image enhancement (Iqbal) method [14] based on color model, and image blur and light absorption (Peng) method [26], successive color correction and superpixel dark channel prior (Lee) method [15]. They are representative in single image dehazing, DCP-based underwater image restoration, underwater image enhancement and underwater image restoration, Lee method [15] is the latest method of underwater image enhancement this year. We tested real underwater images by amateurs and underwater images datasets [1, 2, 19], which include diver image, fish and open scene.

Figure 9 shows the experimental renderings obtained by different algorithms for each underwater scene. As can be seen from Fig. 9a, the poor visibility of the original image is caused by a turbid medium. From Fig. 9b, c, d, e, f and g, we can see that all the six methods can restore the image to a certain extent, and improve the visibility and local details of the image. Although the methods of He [8] and Drews [3] have increased the contrast and details, since the attenuation energy cannot be separately compensated according to different wavelengths, the result after processing shows poor visibility and color distortion, such as the color of Image 5, 6 are dark green, Image 1 has a poor visibility. Peng [26] eliminates the haze in the original underwater image, but the visibility and details are not good enough, for instance, the fish in Image 1 and 2 are not clear. As a classic underwater image enhancement method, the Iqbal [14] method enhances the visibility and color to a certain extent, such as Image 2 and Image 3. However, the underwater imaging model is not considered, so the enhancement result

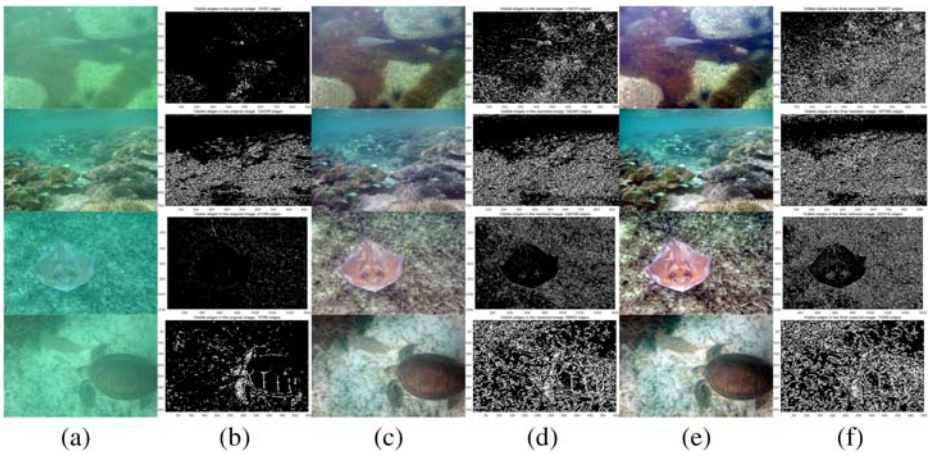

Fig. 8 Contrast stretch (**a**) original image (**b**) The number of visible edges of the original image (**c**)Image before contrast stretch (**d**)the number of visible edges of the image before contrast stretching (**e**)Image after contrast stretch (**f**)the number of visible edges of the image after contrast stretch

can be over-enhanced or under-saturated. For example, the portrait part in Image 6 is over-enhanced, introducing color deviation. Lee [15] enhances the details and eliminates the haze of the original underwater image, but the visibility is not good enough, such as the portrait face in image 5 and image 6 is not clear. Compared with the above method, our method successfully restores the details of the original underwater image, with no deviation in color, more natural and better visual effect.

4.3 Quantitative comparison

There is no confirmed database of underwater images, and different scholar's use different methods to evaluate their methods. In order to verify that the method proposed in this paper has relatively real color, visibility and contrast. The experimental results of different algorithms are quantitatively compared by using objective evaluation metrics, such as information entropy (IE) [32], average gradient (AG) [32], and underwater color image quality evaluation (UCIQE) [28], which are widely used at present.

IE is the average amount of information of an image, which can describe the color richness of the image. *IE* is defined as follows:

$$IE = -\sum_{x=0}^{255} p(x) log_2 p(x) \tag{25}$$

where x is a pixel value, $p(x)$ represents the probability of the occurrence of a pixel x on the whole image. A higher information entropy values indicate the image has richer color information.

AG reflects the change rate of minute details of the image and indicates the relative clarity of the image. *AG* is defined as Eq. (26):

Fig. 9 The results of Qualitative comparison (**a**) Original image of underwater image (**b**)He method [8] (**c**) Drews method [3] (**d**) Iqbal method [14] (**e**) Peng method [26] (**f**) Lee method [15] (**g**) Our image restoration method

$$AG = \frac{1}{(U-1)(V-1)} \sum_{a-1}^{U-1} \sum_{V-1}^{V-1} \sqrt{\frac{(f(a,b)-f(a+1,b))^2 + (f(a,b)-f(a,b+1))^2}{2}} \quad (26)$$

Where, f is the input image, U and V respectively represent the width and height of the input image. A higher average gradient values indicate the image clearer.

UCIQE can be expressed as follows:

$$UCIQE = w_1 \times \sigma_c + w_2 \times con_l + w_3 \times \mu_s \quad (27)$$

where the values of these coefficients are the same as those in reference [28]. UCIQE is a comprehensive metric of the chroma, saturation, and contrast of an image. A bigger UCIQE value means better image quality.

To avoid the deviation of subjective analysis, the objective evaluation metrics is used to make a quantitative comparison of Fig. 9. According to the equation, the information entropy, average gradient and underwater color image quality evaluation metric of Fig. 9 are calculated which showed in Table 2. Table 2 shows that the AG and UCIQE of the image processed by He method [8], Drews method [3], Iqbal method [14], Peng method [26], Lee method [15] and our method are higher than those of the original image. It shows that these methods can enhance the details and visibility of the image, and can balance the chroma, saturation and contrast of the restored image. Except for He, Drews and Lee methods, the IE of other methods is higher than that of the original image, which denotes that the image is rich in color. The IE of Image 5 and 6 processed by He method is lower than that of the original image, which denotes that the processed image lacks color information. The IE of Image 3, 4, 5, 6 processed by Drews method is lower than that of the original image, and also lower than that of He method, after processing image slants color. The IE of Image 4, 5, 6 processed by Lee method is lower than that of the original image, which denotes that the processed image lacks color information. As shown in Table 2, the IE and UCIQE of the method in this paper are all higher than those of other methods. The highest UCIQE value indicates that our restoration method can availably balance the chroma, saturation, and contrast. The best IE indicates rich color information, high average information amount and good visual effect. As shown in Table 2, the AG of this method is lower than Lee method and higher than other methods. The best AG indicates that Lee method effectively enhances image details, but the IE and UCIQE are lower than the method in this paper, indicating that the image visual effect and quality are not good enough. In conclusion, compared with other state-of-the-art methods, the method in this paper effectively enhances image details and color information, improves image quality and visibility, and has a good visual effect.

4.4 Application test

Local feature point matching [21] plays a significant role in many computer vision applications, for example object recognition and detection, object tracking [23]. For the first time, Ancuti and Ancuti [1] used SIFT local feature point matching to evaluate underwater images. We use the SIFT operator to calculate keypoints and compare the keypoints calculation and matching process for a pair of underwater images and the corresponding images restored by our method (see in Fig. 10). In both cases, we used the exact same original implementation of SIFT. In this paper, matched pairs of keypoints increased significantly. This shows that our method does not introduce artifacts, and mainly recovers the global contrast and local features of underwater images. Application test results demonstrate that our method is applicable to computer vision applications.

Table 2 IE, AG, and UCIQE of the proposed algorithm with four other algorithms in Fig. 9

Image		Original	He	Drews	Iqbal	Peng	Lee	Our
Image1	IE	6.682	6.948	7.243	7.411	7.482	7.037	**7.807**
	AG	1.213	1.981	2.499	2.419	1.745	**5.833**	2.574
	UCIQE	0.368	0.519	0.551	0.547	0.527	0.587	**0.639**
Image2	IE	6.907	7.171	7.341	7.458	7.457	7.424	**7.834**
	AG	1.480	2.786	2.886	2.709	2.696	**4.166**	3.993
	UCIQE	0.426	0.547	0.566	0.572	0.578	0.617	**0.664**
Image3	IE	7.277	7.493	6.412	7.500	7.407	7.293	**7.840**
	AG	1.896	3.479	3.292	2.271	3.230	**5.595**	4.148
	UCIQE	0.414	0.514	0.580	0.509	0.523	0.624	**0.634**
Image4	IE	7.564	7.700	6.503	7.294	7.593	7.221	**7.843**
	AG	2.381	3.295	3.663	2.545	2.895	**5.985**	4.256
	UCIQE	0.431	0.544	0.580	0.488	0.471	0.566	**0.614**
Image5	IE	7.599	7.109	6.931	7.605	6.687	6.885	**7.850**
	AG	1.489	1.708	1.951	1.660	1.608	**3.288**	2.300
	UCIQE	0.423	0.482	0.499	0.564	0.556	0.502	**0.639**
Image6	IE	7.261	7.074	6.482	7.639	7.752	6.793	**7.768**
	AG	1.396	1.112	1.052	1.863	2.054	**5.214**	2.488
	UCIQE	0.393	0.426	0.419	0.614	0.578	0.579	**0.701**

5 Conclusion

We propose a method of underwater image restoration based on secondary guided transmission map. Firstly, the red channel is reversed, and the dark channel prior is used on the reversed image to obtain the background light. Then, the rough transmission map is obtained by adding saturation, and the improved guided filter is used to refine the transmission map. And it is combined with the underwater imaging model to restore the image. Finally, auto level processing is carried out on the restored image. Multiple underwater images are used to evaluate the recovery effect of the proposed method and compare it with state-of-the-art

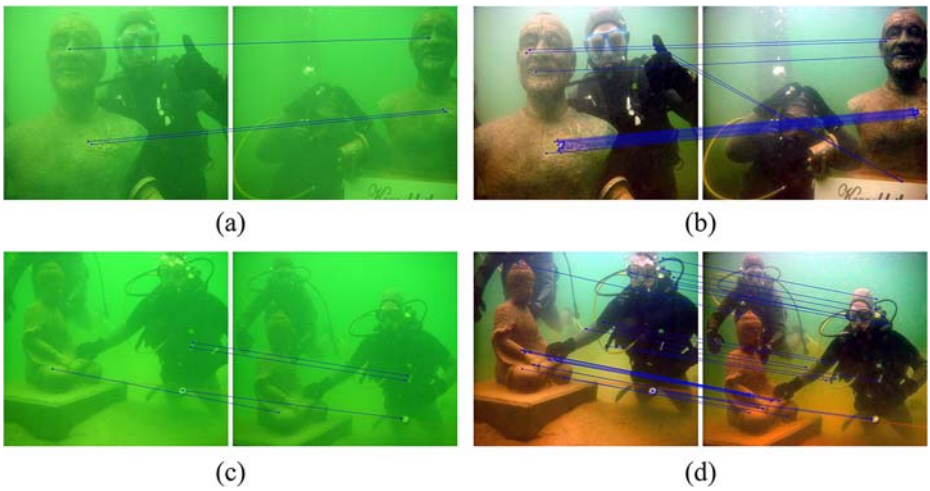

Fig. 10 Local feature points matching (**a**)original image shows 3 valid matches, (**b**) corresponds to (**a**) the processing result of our method shows 22 matches (including 2 mismatches), (**c**) original image shows 4 valid matches, and (**d**) corresponds to (**c**) the restored image of our method shows 32 valid matches

methods. Experimental results show that our method is better than other state-of-the-art methods in both qualitative and quantitative aspects. The method in this paper improves the contrast and enhances the details of the image, realizes the color correction, recovers the image clearly, the visual effect is good.

Although our method has good performance for underwater image restoration, there are some problems. 1) The parameters in this paper are set manually, which is applicable to the image restoration of some scenes. However, some parameters cannot be adjusted adaptively, so satisfactory restoration effects cannot be provided. 2) A simplified underwater optical imaging model is adopted in this paper, the result of restoration at a large depth of field is not ideal due to without considering the effect of forward scattering. Our future work will focus on these issues.

Acknowledgments This work was supported in part by the National Natural Science Foundation of China under Grant 61702074, in part by the Liaoning Provincial Natural Science Foundation of China under Grant 20170520196, in part by the Fundamental Research Funds for the Central Universities under Grant 3132019205, and in part by the Fundamental Research Funds for the Central Universities under Grant 3132019354.

References

1. Ancuti C, Ancuti CO, Haber T, Bekaert P (2012) Enhancing underwater images and videos by fusion. In: proceedings of Proc IEEE Conf Comput Vis Pattern Recognit (CVPR), pp 81–88
2. Chiang JY, Chen YC (2012) Underwater image enhancement by wavelength compensation and Dehazing. IEEE Trans Image Process 21(4):1756–1769
3. Drews-Jr P, Nascimento E, Moraes F, Botelho S, Campos M (2013) Transmission estimation in underwater single images. In: proceedings of IEEE international conference on computer vision workshops (ICCVW), pp 825–830
4. Galdran A, Pardo D, Picón A, Alvarez-Gila A (2015) Automatic Red-Channel underwater image restoration. J Vis Commun Image Represent 26:132–145
5. Garg D, Garg NK, Kumar M (2018) Underwater image enhancement using blending of CLAHE and percentile methodologies. Multimed Tools Appl 77(20):26545–26561
6. Hautière N, Tarel JP, Aubert D, Dumont É (2008) Blind contrast restoration assessment by gradient Ratioing at visible edges. Image Anal Stereol, vol 27:87–95
7. He D, Seet G (2004) Divergent-beam LiDAR imaging in turbid water. Opt Lasers Eng 41(1):217–231
8. He K, Sun J, Tang X (2011) Single image haze removal using dark channel prior. IEEE Trans Pattern Anal Mach Intell 33(12):2341–2353
9. He K, Sun J, Tang X (2013) Guided image filtering. IEEE Trans Softw Eng 35(6):1397–1409
10. Hou W, Gray D, Weidemann A, Arnone R (2008) Comparison and validation of point spread models for imaging in natural waters. Opt Express 16(13):9958–9965
11. Hu H, Zhao L, Li X, Wang H, Liu T (2018) Underwater image recovery under the non-uniform optical field based on polarimetric imaging. IEEE photon J, vol 10(1). https://doi.org/10.1109/JPHOT.2018.2791517
12. Huang Y, Ding W, Li H (2017) Haze removal method for UAV reconnaissance images based on image enhancement. J Beijing Univ Aeronaut Astronaut 43(3):592–601 in Chinese. https://doi.org/10.13700/j.bh.1001-5965.2016.0169.html
13. Huang B, Liu T, Hu H, Han J, Yu M (2016) Underwater image recovery considering polarization effects of objects. Opt Express 24(9):9826–9838
14. Iqbal K, Salam RA, Osman A, Talib AZ (2007) Underwater image enhancement using an integrated color model. IAENG Int J Comput Sci (IJCS) 32(2):239–244
15. Lee HS, Moon SW, Eom IK (2020) Underwater image enhancement using successive color correction and Superpixel Dark Channel prior. Symmetry 12(8):1220
16. Levin A, Lischinski D, Weiss Y (2007) A closed form solution to natural image matting. IEEE Trans Pattern Anal Mach Intell 30(2):228–242

17. Li C, Guo J, Chen S, Tang Y, Pang Y, Wang J (2016) Underwater image restoration based on minimum information loss principle and optical properties of underwater imaging. In: Proceedings of IEEE international conference on image processing (ICIP), pp 1993–1997
18. Li C, Guo J, Cong R, Pang Y, Wang B (2016) Underwater image enhancement by dehazing with minimum information loss and histogram distribution prior. IEEE Trans Image Process 25(12):5664–5677
19. Li C, Guo C, Ren W, Cong R, Hou J, Kwong S, Tao D (2019) An underwater image enhancement benchmark dataset and beyond. IEEE Trans Image Process 29:4376–4389
20. Li J, Li Y (2018) Guided local laplacian filter-based image enhancement for deep-sea sensor networks. Multimed Tools Appl 77(9):10823–10834
21. Lowe D (2004) Distinctive image features from scale-invariant keypoints. Int J Comput Vis 60(2):91–110
22. Lu X, Guo Y, Liu N, Wan L, Fang T (2018) Non-convex joint bilateral guided depth upsampling. Multimed Tools Appl 77:15521–15544
23. Lu X, Ni B, Ma C, Yang X (2019) Learning transform-aware attentive network for object tracking. Neurocomputing 349(JUL.15):133–144
24. Mathias A, Samiappan D (2019) Underwater image restoration based on diffraction bounded optimization algorithm with dark channel prior. Opt Int J Light Electron Opt 192:162925
25. McGlamery B (1980) A computer model for underwater camera systems. Proc SPIE 208:221–231
26. Peng Y, Cosman P (2017) Underwater image restoration based on image blurriness and light absorption. IEEE Trans Image Process 26(4):1579–1594
27. Wen H, Tian Y, Huang T, Gao W (2013) Single underwater image enhancement with a new optical model. In: Proceedings of IEEE International Symposium on Circuits and Systems (ISCAS), pp:753–756
28. Yang M, Sowmya A (2015) An underwater color image quality evaluation metric. IEEE Trans Image Process 24(12):6062–6071
29. Yang M, Sowmya A, Wei Z, Zheng B (2019) Offshore underwater image restoration using reflection-decomposition-based transmission map estimation. IEEE J Ocean Eng, pp 1-13. https://doi.org/10.1109/JOE.2018.2886093
30. Zhao X, Jin T, Qu S (2015) Deriving inherent optical properties from background color and underwater image enhancement. Ocean Eng 94:163–172
31. Zhou J, Zhang D, Zhang W (2020) The classical and state-of-the-art approaches for underwater image defogging: a comprehensive survey. Front Inform technol Electron Eng. https://doi.org/10.1631/FITEE.2000190
32. Zhou J, Zhang D, Zou P, Zhang W, Zhang W (2019) Retinex-based Laplacian pyramid method for image defogging. IEEE Access 7:122459–122472